A Comparative Study of Four Feedback Linearization Schemes for Motion Planning of Fixed-Wing Unmanned Aerial Vehicles

Hossein Bonyan Khamseh[1]

ABSTRACT: In this paper, different feedback linearization schemes are studied to address the motion planning problem of fixed-wing unmanned aerial vehicles. For a unmanned aerial vehicle model with second-order dynamics, several schemes are studied to make the vehicle (i) fly over and (ii) make a loitering around the objective position. For each scheme, comparisons are made to illustrate the advantages and disadvantages. Lyapunov stability analysis is used to prove the stability of the proposed schemes, and simulation results for some case studies are included to show their feasibility.

KEYWORDS: Feedback linearization, Unmanned aerial vehicle, Motion planning.

INTRODUCTION

In recent years, unmanned aerial vehicles (UAVs) have gained increasing attention for various missions such as remote sensing of agricultural products (Costa *et al.* 2012), forest fire monitoring (Casbeer *et al.* 2006), search and rescue (Almurib *et al.* 2011), transmission line inspection (Li *et al.* 2013) and border monitoring (Beard *et al.* 2006). To this date, various approaches have been employed to address the motion planning of UAVs to reach, fly over or loiter around an objective position. As an example, in Frew *et al.* (2008) and Lawrence *et al.* (2008), vector fields with a stable limit cycle centered on the target position were constructed. In the mentioned studies, the authors employed a Lyapunov vector field guidance (LVFG) law to bring the UAV to an observation "orbit" around the target. Also, in Gonçalves *et al.* (2011), a vector field approach was used to bring several non-holonomic UAVs to a static curve embedded in the 3-D space. In Gonçalves *et al.* (2010), vector fields were determined such that a robot converged to a time-varying curve in n-dimensions and circulated it. In Hsieh *et al.* (2008), decentralized controllers were proposed to bring a number of robotic agents to generate desired simple planar curves, while avoiding inter-agent collision. In Hsieh *et al.* (2007), the controllers were modified such that the robots converged to a star-shaped pattern and, once on the objective curve, circulated it. In Bonyan Khamseh *et al.* (2014), based on the concept of flight corridor, a decentralized coordination strategy was proposed to bring a team of fixed-wing UAVs to a circular orbit, while avoiding inter-UAV collision. In Hafez *et al.* (2013), model predictive control was used to create a

1. Universidade Federal de Minas Gerais – Escola de Engenharia Elétrica – Departamento de Engenharia Elétrica – Belo Horizonte/MG – Brazil.

Author for correspondence: Hossein Bonyan Khamseh | Universidade Federal de Minas Gerais - Escola de Engenharia Elétrica - Departamento de Engenharia Elétrica Av. Pres. Antônio Carlos, 6627 – CEP: 31 270-901 – Pampulha - Belo Horizonte/MG – Brazil | Email: h.bonyan@gmail.com

dynamic circular formation around a given target. By means of simulations, it was shown that the system was stable, but formal stability analysis was not provided. In Marasco *et al.* (2012), the same approach was improved to address encirclement of multiple targets, without stability analysis.

It is also possible to employ feedback linearization to simplify the equations of motion in motion planning problems (Lawton *et al.* 2003; Fan and Zhiyong 2009; Kanchanavally *et al.* 2006). As an example, in Lawton *et al.* (2003), feedback linearization was employed to study the formation control of the end-effector position of a team of non-holonomic robots. Having obtained simpler double-integrator equations, control laws were designed and formation control was achieved. Stability of the system was proven by means of Lyapunov stability theory. In Fan and Zhiyong (2009), for a multi-agent system, the authors proposed a dynamic feedback linearization scheme to describe the equations of motion of each agent by third-order integrators. Then, a formation control law with inter-agent damping was developed, and asymptotic stability of the system was verified using Lyapunov stability analysis. In Kanchanavally *et al.* (2006), the specific problem of 3-D motion planning of UAVs via feedback linearization was studied. In that study, a non-holonomic UAV equipped with a fixed-angle camera was considered. The footprint of the camera was defined as the system output, and it was shown that it converged to an objective position. Similar to the previous papers (Lawton *et al.* 2003; Fan and Zhiyong 2009), the stability of the system was studied by means of Lyapunov stability theory. Yet, an important drawback of Kanchanavally *et al.* (2006) is that it did not include the constraints of minimum and maximum forward velocity of fixed-wing UAVs. Therefore, the UAVs came to rest, i.e. zero forward velocity, once the camera footprint converged to the target position.

In this paper, several feedback linearization schemes are studied to address the problem of motion planning of fixed-wing UAVs flying with constant forward velocity. The objective here is that the UAV (i) flies over or (ii) loiter around a static objective position, without coming to rest.

FEEDBACK LINEARIZATION SCHEMES

In the following subsections, a UAV with an on-board camera will be considered. For a fixed-angle forward-looking camera, the results were presented in Kanchanavally *et al.* (2006), where the UAV finally came to rest. Due to minimum

forward velocity constraint, that method is not applicable to fixed-wing UAVs. Here, we define several schemes such that the footprint of the on-board camera converges to an objective position while the UAV either flies over or loiters around the objective position with constant forward velocity.

UAV WITH FORWARD-LOOKING CAMERA, SCHEME #1

In the first scheme a fixed-wing UAV with variable-angle forward-looking camera is considered. In the control affine form, considering a simplified rigid-body model, the dynamic equations of motion of the system are given by:

$$
\begin{bmatrix} \dot{x}_1 \\ \dot{x}_2 \\ \dot{x}_3 \\ \dot{x}_4 \\ \dot{x}_5 \\ \dot{x}_6 \\ \dot{x}_7 \\ \dot{x}_8 \end{bmatrix} = \begin{bmatrix} \dot{r}_x \\ \dot{r}_y \\ \dot{\theta} \\ \dot{\omega} \\ \dot{r}_z \\ \dot{v}_z \\ \dot{\phi} \\ \dot{v}_\phi \end{bmatrix} = \begin{bmatrix} v\cos x_3 \\ v\sin x_3 \\ x_4 \\ 0 \\ x_6 \\ 0 \\ x_8 \\ 0 \end{bmatrix} + \begin{bmatrix} 0 & 0 & 0 \\ 0 & 0 & 0 \\ 0 & 0 & 0 \\ \frac{1}{I} & 0 & 0 \\ 0 & 0 & 0 \\ 0 & \frac{1}{m} & 0 \\ 0 & 0 & 0 \\ 0 & 0 & \frac{1}{J} \end{bmatrix} \begin{bmatrix} u_1 \\ u_2 \\ u_3 \end{bmatrix} = \boldsymbol{f} + g\boldsymbol{u} \quad (1)
$$

where: r_x, r_y and r_z represent x, y, and z positions of the UAV; v and v_z represent the constant velocity v in the $x - y$ horizontal plane and the velocity v_z in the z-direction; θ and ω represent the heading angle and angular velocity of the UAV; ϕ and v_ϕ represent the angle and angular speed of the camera, respectively. The UAV constants are given by m (UAV mass), I (UAV moment of inertia about z-axis) and J (camera moment of inertia about its rotation axis). The input vector is $\boldsymbol{u} = [u_1\ u_2\ u_3]^{\mathrm{T}}$.

In the model given by Eq. 1, it has been assumed that the forward velocity in the $x - y$ plane, i.e. v, is constant. With this simplification, if one initially chooses the forward velocity to satisfy $v_{min} \le v \le v_{max}$, one can conclude that the minimum and maximum forward velocity constraints will be automatically satisfied throughout the mission. Also, since the camera is not mounted with a fixed angle, one can come up with scenarios in which the UAV does not come to rest when the camera footprint converges to the objective position. As it can be seen from Eq. 1, the camera dynamics has been assumed to be second-order and completely decoupled from the UAV dynamics. For a forward-looking camera, one can consider the following output for the system (Kanchanavally *et al.* 2006):

$$\boldsymbol{\Gamma} = \begin{bmatrix} x_1 + L\cos x_3 \\ x_2 + L\sin x_3 \\ x_5 \end{bmatrix}, \tag{2}$$

where: $L = r_z\cot\phi$.

As schematically shown in Fig. 1, the first two elements of Γ represent x and y positions of the footprint of the forward-looking camera. Also, the third element represents the altitude of the UAV. An important advantage of this scheme, compared to Kanchanavally *et al.* (2006), is that ϕ is not constant here and is considered one of the system state variables.

Assuming relative degree of r_i for the i-th elements of Γ, after r_i times differentiation, one finds:

$$\begin{bmatrix} \Gamma_1^{(r_1)} \\ \Gamma_2^{(r_2)} \\ \Gamma_3^{(r_3)} \end{bmatrix} = \begin{bmatrix} L_f^{r_1}\Gamma_1 + \sum_{i=1}^{3} L_{g_i}(L_f^{r_1-1}\Gamma_1)u_i \\ L_f^{r_2}\Gamma_2 + \sum_{i=1}^{3} L_{g_i}(L_f^{r_2-1}\Gamma_2)u_i \\ L_f^{r_3}\Gamma_3 + \sum_{i=1}^{3} L_{g_i}(L_f^{r_3-1}\Gamma_3)u_i \end{bmatrix} = \boldsymbol{A} + \boldsymbol{Bu} \tag{3}$$

where: $L_f\Gamma_i$ is the Lie derivative, i.e. $L_f\Gamma_i = \partial\Gamma_i/\partial x$ and g_i is the i-th column of the matrix g. Also, $\boldsymbol{A} \in \boldsymbol{R}^{3\times1}$ and $\boldsymbol{B} \in \boldsymbol{R}^{3\times3}$, where the elements of $\boldsymbol{A}$ are given below. For the system given by Eq. 1 and with output given by Eq. 2, one can obtain the vector of relative degree as $[r_1\ r_2\ r_3] = [2\ 2\ 2]$.

$$A_1 = -vx_4\sin x_3 - 2x_6x_8\frac{1}{\sin^2 x_7}\cos x_3 +$$

$$+ 2x_5(x_8)^2\frac{\cos x_7}{\sin^3 x_7}\cos x_3 - 2x_6\cot x_7\, x_4\sin x_3 +$$

$$+ 2x_5x_8\frac{1}{\sin^2 x_7}x_4\sin x_3 - L(x_4)^2\cos x_3$$

$$A_2 = vx_4\cos x_3 - 2x_6x_8\frac{1}{\sin^2 x_7}\sin x_3 +$$

$$+ 2x_5(x_8)^2\frac{\cos x_7}{\sin^3 x_7}\sin x_3 + 2x_6\cot x_7\, x_4\cos x_3 -$$

$$- 2x_5x_8\frac{1}{\sin^2 x_7}x_4\cos x_3 - L(x_4)^2\sin x_3$$

and $A_3 = 0$.
Also:

$$B = \begin{bmatrix} \dfrac{-L}{I}\sin x_3 & \dfrac{1}{m}\cot x_7\cos x_3 & -\dfrac{1}{J}\dfrac{x_5}{\sin^2 x_7}\cos x_3 \\[2ex] \dfrac{L}{I}\cos x_3 & \dfrac{1}{m}\cot x_7\sin x_3 & -\dfrac{1}{J}\dfrac{x_5}{\sin^2 x_7}\sin x_3 \\[2ex] 0 & \dfrac{1}{m} & 0 \end{bmatrix}$$

One can verify that $\det(B) = -(x_5)^2\cos x_7/m\cdot I\cdot J\sin^3 x_7$. This determinant can be zero if $x_5 = 0$ or $\cos x_7 = 0$. In order to show that $x_5 \neq 0$, we define the error as:

$$\boldsymbol{E} = (\boldsymbol{\Gamma} - \boldsymbol{R}) + (\dot{\boldsymbol{\Gamma}} - \dot{\boldsymbol{R}}) \tag{4}$$

where: $\boldsymbol{R}$ is the reference signal and, for a stationary reference signal, one will have $\dot{\boldsymbol{R}} = 0$. Assuming $E_3(0) > -R_3$, one can rewrite the third row of Eq. 4 as:

$$\dot{\Gamma}_3 = -\Gamma_3 + \underbrace{(E_3 + R_3)}_{u'} \tag{5}$$

Therefore:

$$\Gamma_3(t) = e^{-t}\Gamma_3(0) + \int_0^t e^{-(t-\tau)}u'(\tau)d\tau \tag{6}$$
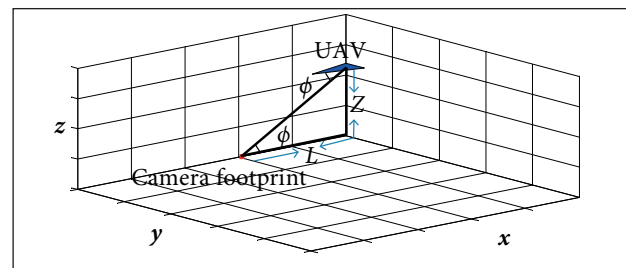

Figure 1. The UAV and its camera footprint in scheme #1.

In the following paragraphs it will be shown that the absolute value of E_3 monotonically decreases and converges to zero. Therefore, noting that $R_3 > 0$, it will be easy to see that $u'(t)$ is always positive. With $\Gamma_3(0) > 0$, from Eq. 6, one can conclude that $\Gamma_3(t) > 0$ and therefore $x_5 \neq 0$, i.e. the altitude cannot be zero. Also, for $\cos x_7 = 0$, one must have $x_7 = kn + \pi/2$. It means that the objective position is exactly underneath the UAV actual position. This is an important drawback which can lead to the failure of this scheme. Yet, due to discretization, control errors and other real-world phenomena, this is not a concern in practical situations. In our simulations, no problem was encountered due to this drawback. Also, $\det(B) \to \infty$ if $x_7 \to k\pi$. Yet, $x_7 \to k\pi$ means that $L \to \infty$. In practice, it is not a legitimate concern because $\Gamma_3(0) > 0$ and also the UAV cannot be infinitely far from its target ($x_7 \neq k\pi$). Therefore it is concluded that $\det(B) = -(x_5)^2\cos x_7/m\cdot I\cdot J\sin^3 x_7 \neq 0$ for practical applications.

In order to study the error dynamics, we differentiate Eq. 4 to obtain:

$$\dot{E} = \dot{\Gamma} + \ddot{\Gamma} = \dot{\Gamma} + A + Bu \qquad (7)$$

Similar to Kanchanavally *et al.* (2006), if we define $u = B^{-1}(-A - \dot{\Gamma} + v)$ and , it is easy to see that:

$$\dot{E} = KE \qquad (8)$$

where: $K \in R^{3\times3}$ and eigenvalues of K have negative real parts.

In order to study the error dynamics given by Eq. 8, one may consider the following Lyapunov function:

$$V = \frac{1}{2} E^T E \qquad (9)$$

The time derivative of the above positive definite V is given by:

$$\dot{V} = \dot{E}^T E = E^T K^T E < 0 \qquad (10)$$

Therefore the error converges to zero. Regarding the internal dynamics with a vector of relative degree of [2 2 2], one needs to propose two more transformations to complete the diffeomorphism. The internal dynamics is given by Eq. 11:

$$\begin{cases} \eta_7 = x_3 \rightarrow \dot{\eta}_7 = x_4 \\ \eta_8 = x_4 \rightarrow \dot{\eta}_8 = \frac{1}{I} u_1 \end{cases} \qquad (11)$$

For a UAV with a forward-looking camera, the only possible motion where the error goes to zero is when the UAV flies on a straight line over the objective position. Therefore, as $t \rightarrow \infty$, $x_4 \rightarrow 0$. With $x_4 \rightarrow 0$, it is easy to conclude that x_3 will be bounded and therefore it is not going to cause undesirable effects. Simulation results verifying the feasibility of this approach will be given in "Simulations" section.

UAV WITH SIDE-LOOKING CAMERA, SCHEME #2

In this subsection, a UAV with variable-angle side-looking camera is considered. The equations of motion of this configuration are identical to those given in Eq. 1 and therefore are not repeated here. For a side-looking camera, the output is given by:

$$\Gamma = \begin{bmatrix} x_1 + L \sin x_3 \\ x_2 - L \cos x_3 \\ x_5 \end{bmatrix} \qquad (12)$$

where the first two elements of Γ represent x and y positions of the footprint of the camera (see Fig. 2).
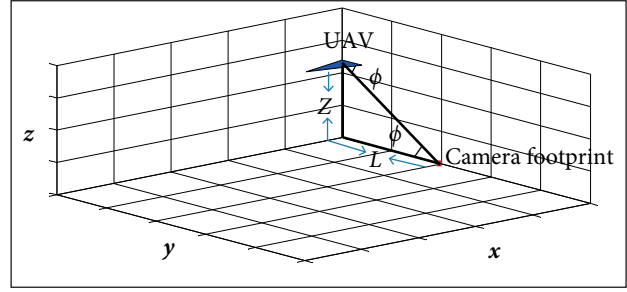

Figure 2. The UAV and its camera footprint in scheme #2.

For the given output, one can verify that $[r_1\ r_2\ r_3] = [2\ 2\ 2]$. Therefore, an equation identical to that given in Eq. 3 is obtained, in which:

$$A_1 = -vx_4 \sin x_3 - 2x_6 x_8 \frac{1}{\sin^2 x_7} \sin x_3 +$$
$$+ 2x_5(x_8)^2 \frac{\cos x_7}{\sin^3 x_7} \sin x_3 + 2x_6 \cot x_7 x_4 \cos x_3 -$$
$$- 2x_5 x_8 \frac{1}{\sin^2 x_7} x_4 \cos x_3 - L(x_4)^2 \sin x_3$$

$$A_2 = vx_4 \cos x_3 + 2x_6 x_8 \frac{1}{\sin^2 x_7} \cos x_3 -$$
$$- 2x_5(x_8)^2 \frac{\cos x_7}{\sin^3 x_7} \cos x_3 + 2x_6 \cot x_7 x_4 \sin x_3 -$$
$$- 2x_5 x_8 \frac{1}{\sin^2 x_7} x_4 \sin x_3 + L(x_4)^2 \cos x_3$$

$$A_3 = 0$$

$$B = \begin{bmatrix} \frac{L}{I}\cos x_3 & \frac{1}{m}\cot x_7 \sin x_3 & -\frac{1}{J}\frac{x_5}{\sin^2 x_7}\sin x_3 \\ \frac{L}{I}\sin x_3 & -\frac{1}{m}\cot x_7 \cos x_3 & \frac{1}{J}\frac{x_5}{\sin^2 x_7}\cos x_3 \\ 0 & \frac{1}{m} & 0 \end{bmatrix}$$

One can verify that $\det(B) = -(x_5)^2 \cos x_7 / m \cdot I \cdot J \sin^3 x_7$. This determinant can be zero if $x_5 = 0$ or $\cos x_7 = 0$. With the reasoning given in the previous subsection (see Eqs. 4 – 6), one can conclude that $x_5 \neq 0$, i.e. the altitude cannot be zero. For a UAV with constant forward velocity and a side-looking camera, the only possible motion where the error goes to zero is when the UAV loiters around the objective position, with a fixed loitering radius. Therefore, with a non-zero loitering radius, it is easy to conclude that $\cos x_7 \neq 0$. Also, $\det(B) \rightarrow \infty$ if $x_7 \rightarrow k\pi$. Yet, $x_7 \rightarrow k\pi$

means that $L \to \infty$, which is not common in practical scenarios. Therefore, it is concluded that $\det(B) = -(x_5)^2 \cos x_7 / m \cdot I \cdot J \sin^3 x_7 \neq 0$ for practical applications, and thus the system given by Eq. 1 with output given by Eq. 12 is input-output linearizable.

For this scheme, the Lyapunov stability analysis is identical to that given by Eqs. 7 – 10. Therefore, it can be concluded that the error dynamics asymptotically converges to zero. Regarding the internal dynamics with a vector of relative degree of [2 2 2], one needs to propose two more transformations to complete the diffeomorphism. The internal dynamics is given by and in Eq. 13:

$$\begin{cases} \eta_7 = x_3 \;\to\; \dot{\eta}_7 = x_4 \\ \eta_8 = x_4 \;\to\; \dot{\eta}_8 = \frac{1}{I} u_1 \end{cases} \tag{13}$$

For a UAV loitering around a given objective position with constant (finite) forward velocity, x_4 will be bounded and cannot go to infinity. Also, in a loitering motion, x_3, i.e. the heading angle, can be shown by $2k\pi + \theta'$ where θ' is a finite value and therefore the internal dynamics will not cause undesirable effects in our approach. Simulation results regarding this scheme will be given in "Simulations" section.

An important drawback of this method is that one cannot explicitly control the final loitering radius of the UAV. Therefore, in the next scheme, we try to explicitly define the loitering radius as one of the system outputs.

UAV WITH SIDE-LOOKING CAMERA, SCHEME #3

In this section, we modify the equations of motion given in Eq. 1 in a manner that a new useful scheme is obtained. In the control affine form, the new dynamic equations of motion are given by Eq. 14:

$$\begin{bmatrix} \dot{x}_1 \\ \dot{x}_2 \\ \dot{x}_3 \\ \dot{x}_4 \\ \dot{x}_5 \\ \dot{x}_6 \\ \dot{x}_7 \\ \dot{x}_8 \end{bmatrix} = \begin{bmatrix} \dot{r}_x \\ \dot{r}_y \\ \dot{\theta} \\ \dot{\omega} \\ \dot{r}_z \\ \dot{v}_z \\ \dot{L} \\ \ddot{L} \end{bmatrix} = \begin{bmatrix} v\cos x_3 \\ v\sin x_3 \\ x_4 \\ 0 \\ x_6 \\ 0 \\ x_8 \\ 0 \end{bmatrix} + \begin{bmatrix} 0 & 0 & 0 \\ 0 & 0 & 0 \\ 0 & 0 & 0 \\ \frac{1}{I} & 0 & 0 \\ 0 & 0 & 0 \\ 0 & \frac{1}{m} & 0 \\ 0 & 0 & 0 \\ 0 & 0 & 1 \end{bmatrix} \begin{bmatrix} u_1 \\ u_2 \\ u_3 \end{bmatrix} = f + gu \tag{14}$$

Here, the main difference is that L and $\dot{L}$ are explicitly considered to be state variables. One may define the system output as:

$$\boldsymbol{\Gamma} = \begin{bmatrix} x_1^2 + x_2^2 \\ x_5 \\ x_7 \end{bmatrix} \tag{15}$$

where the first element of Γ is the square of the distance of the UAV from the origin of the coordinate system, i.e. the stationary objective position.

It can be readily seen that $[r_1 \; r_2 \; r_3] = [3\;2\;2]$. Therefore, in a compact form, one can write:

$$\begin{bmatrix} \dddot{\Gamma}_1 \\ \ddot{\Gamma}_2 \\ \ddot{\Gamma}_3 \end{bmatrix} = A + Bu \tag{16}$$

where:

$$A = \begin{bmatrix} -2vx_4^2(x_1\cos x_3 + x_2 \sin x_3) \\ 0 \\ 0 \end{bmatrix},$$

$$B = \begin{bmatrix} \frac{-2v}{I}(x_1\sin x_3 - x_2\cos x_3) & 0 & 0 \\ 0 & \frac{1}{m} & 0 \\ 0 & 0 & 1 \end{bmatrix}$$

One can verify that $\det(B) = -2v_c/m \cdot I \,(x_1 \sin x_3 - x_2 \cos x_3)$. An important disadvantage is that this determinant can be zero if $x_1 \sin x_3 - x_2 \cos x_3 = 0$, i.e. when the UAV is either flying radially inward or radially outward. Yet, if the heading of the UAV does not fall within this region, the UAV can converge to a loitering motion around the origin of the coordinate system. On the other hand, the advantage of this scheme is that, depending on the value of R_1, i.e. the first element of the reference signal, one can come up with scenarios in which the UAV converges to a loitering radius either smaller or greater than the initial one. Also, a second advantage is that one can explicitly control L, as R_3. Therefore, for $R_3 < 2\sqrt{R_1}$, $R_3 = 22\sqrt{R_1}$ and $R_3 > 2\sqrt{R_1}$, one can define scenarios in which the UAV loiters around the origin while the camera footprint sweeps a circle with the radius smaller than, equal to or greater than $\sqrt{R_1}$. This is schematically shown in Figs. 3a to 3c.

Regarding the stability of the system, if we define the error as:

$$\begin{bmatrix} E_1 \\ E_2 \\ E_3 \end{bmatrix} = \left(\begin{bmatrix} \Gamma_1 \\ \Gamma_2 \\ \Gamma_3 \end{bmatrix} - \begin{bmatrix} R_1 \\ R_2 \\ R_3 \end{bmatrix} \right) + \left(\begin{bmatrix} \ddot{\Gamma}_1 \\ \dot{\Gamma}_2 \\ \dot{\Gamma}_3 \end{bmatrix} - \begin{bmatrix} \ddot{R}_1 \\ \dot{R}_2 \\ \dot{R}_3 \end{bmatrix} \right) \tag{17}$$

for a stationary reference signal, one will have $\dot{R} = \ddot{R} = 0$. Differentiating Eq. 17, one has:

$$\begin{bmatrix} \dot{E}_1 \\ \dot{E}_2 \\ \dot{E}_3 \end{bmatrix} = \begin{bmatrix} \dot{\Gamma}_1 \\ \dot{\Gamma}_2 \\ \dot{\Gamma}_3 \end{bmatrix} + \begin{bmatrix} \ddot{\Gamma}_1 \\ \ddot{\Gamma}_2 \\ \ddot{\Gamma}_3 \end{bmatrix} \qquad (18)$$

Now, if we define $u = B^{-1}(-A - \dot{\Gamma} + v)$ and $v = KE$, it is easy to see that:

$$\dot{E} = KE \qquad (19)$$

where: K is a matrix with eigenvalues which have negative real parts.

In order to study the error dynamics given by Eq. 19, one may consider the following Lyapunov function:

$$V = \frac{1}{2}E^T E \qquad (20)$$

The time derivative of the above positive definite V is given by:

$$\dot{V} = \dot{E}^T E = E^T K^T E < 0 \qquad (21)$$
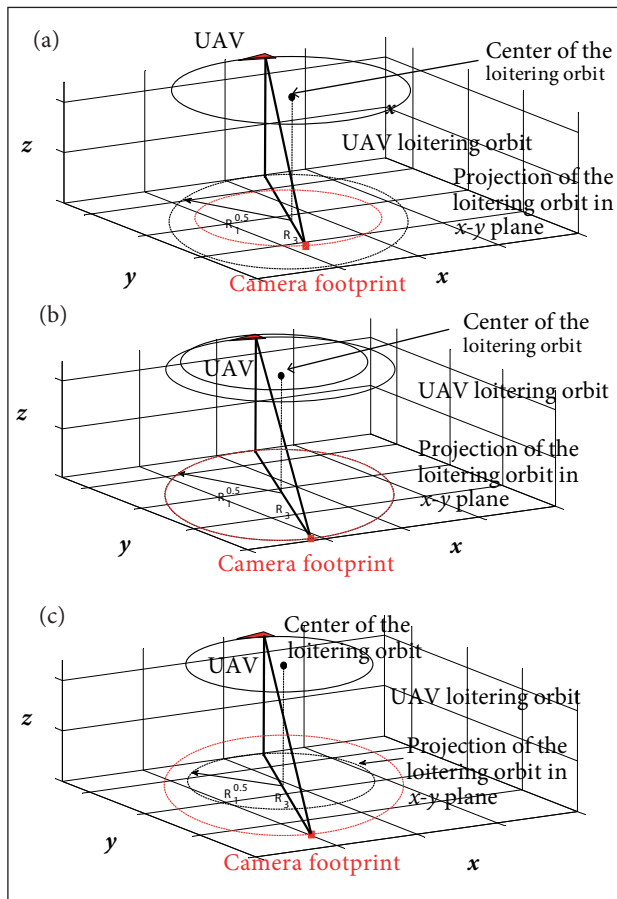
Figure 3. Three different scenarios in scheme #3.

Therefore the error dynamics is asymptotically stable. Regarding the internal dynamics with a vector of relative degree of [3 2 2], one needs to propose one more transformation to complete the diffeomorphism. The internal dynamics is given by $\dot{\eta}_8$ in Eq. 22:

$$\eta_8 = x_4 \; \rightarrow \; \dot{\eta}_8 = \frac{1}{l}u_1 \qquad (22)$$

For a UAV loitering around a given objective position with constant (finite) forward velocity, x_4 will be bounded and cannot go to infinity. Therefore, the internal dynamics will not cause undesirable effects in our approach. Simulation results regarding this scheme will be given in "Simulations" section.

UAV WITH SIDE-LOOKING CAMERA AND ONE VIRTUAL FORWARD-LOOKING CAMERA, SCHEME #4

In this subsection, we modify the previous scheme in the sense that the UAV can loiter around the origin with a desirable radius while avoiding the singularity problem of scheme #3. Convergence to a loitering radius (i) smaller or (ii) greater than the initial radius is studied separately.

Convergence to a Loitering Radius Smaller than the Initial One

In this scenario, it is initially assumed that the UAV is equipped with a virtual forward-looking camera. From geometry, one can find two tangent lines (and their corresponding tangency points) between the initial position of the UAV and the circle with the reference radius. In the first phase, the UAV can choose one of the tangency points as its virtual objective position and fly over it, according to scheme #1, discussed earlier. Assuming that the UAV flies over the tangent line, its heading will be perpendicular to the radius of the objective circle as it reaches the virtual objective position. As the UAV reaches the tangency point, it switches to scheme #3. The advantage here is that, in the second phase, it is ensured that the heading of the UAV is far from inward-outward direction and therefore scheme #3 can bring the UAV to loiter around the objective position, with desirable radius. This is schematically shown in Fig. 4.

The details of feedback linearization, control laws and stability analysis of scheme #1 and scheme #3 were discussed in the previous subsections and are not repeated here. Simulation results of this scheme will be given in "Simulations" section.
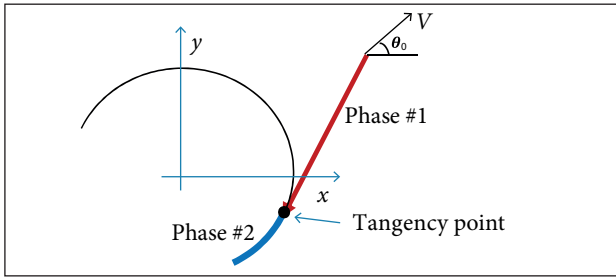
Figure 4. Scheme #3, convergence to a loitering radius smaller than the initial one.

Convergence to a Loitering Radius Greater than the Initial One

Similar to the previous subsection, we assume that the UAV is equipped with a virtual forward-looking camera and a side-looking camera. The scenario proposed here consists of three phases, as shown in Fig. 5.
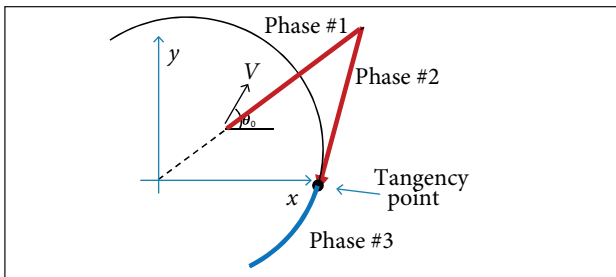

Figure 5. Scheme #3, convergence to a loitering radius greater than the initial one.

In the first phase, based on scheme #1, the UAV flies to a virtual objective position which is on the extension of the line connecting the origin to the initial position of the UAV. Let's denote the UAV distance from the origin by d and the desired loitering radius by R^*. At the end of the first phase, when d is relatively greater than R^*, the UAV finds the tangent lines from its current position to the circle with the radius R^*. With d relatively greater than R^*, one can assume that, in the second phase, based on scheme #1, the UAV flies on the tangent line to reach the tangency point (second virtual objective position). Once at this point, the UAV has reached the reference radius and switches to scheme #3. In the third phase, based on scheme #3, the UAV loiters around the origin with $R_1 = R^*$. The details of feedback linearization, control laws and stability analysis of scheme #1 and scheme #3 were discussed in the previous subsections and are not repeated here. Simulation results of this scheme will be given in "Simulations" section.

SIMULATIONS

In this section, some case studies are developed to verify the feasibility of the proposed schemes. A light fixed-wing UAV is considered, with its characteristics given in Table 1. In the simulations, where applicable, the initial condition of the UAV is assumed to be $[-1{,}800 \text{ m} \ \ 2{,}500 \text{ m} \ \ 240 \text{ deg} \ \ 1 \text{ deg/s} \ \ 300 \text{ m} \ \ 10 \text{ m/s} \ \ 10 \text{ deg} \ \ 1 \text{ deg/s}]^T$. For the first scheme, the reference signal is assumed to be $[100 \text{ m} \ \ -20 \text{ m} \ \ 500 \text{ m}]^T$. For the described case study, simulations were carried out and the results are shown in Fig. 6.

As it can be readily seen from Fig. 6, after the initial transition, the UAV has aligned its motion such that it flies almost over the objective position on a straight line. Once on this line, the objective position is monitored by merely controlling the angle of the camera (see Fig. 7).

As it was expected, in this scheme, the camera angle will approach zero as the UAV flies toward the objective position. As the UAV flies away from the objective position, the camera angle will approach π, as $t \to \infty$.

Table 1. Characteristics of the light fixed-wing UAV.

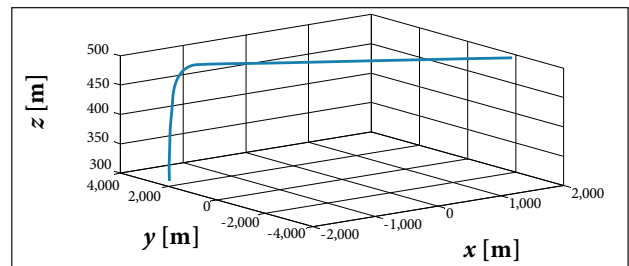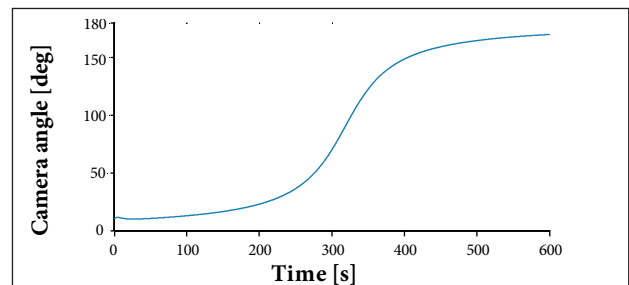| Mass (kg)	Moment of inertia — z-axis (kg·m²)	Moment of inertia of the camera (kg·m²)	Forward velocity (m/s)
1	0.01	0.001	10

Figure 6. UAV trajectory obtained from scheme #1.

Figure 7. Forward-looking camera angle obtained from scheme #1.

For the second scheme, the reference signal is assumed to be [−50 m −50 m 500 m]^T. For the described case study, simulations were carried out and the results are shown in Fig. 8.

As it can be seen from Fig. 8, the UAV has successfully converged to a loitering motion around the objective position. Also, as expected, the camera angle converges to a fixed value in the loitering motion (see Fig. 9).

The initial conditions of the third scheme are assumed to be identical to those of the first scheme. Here, the reference signal is assumed to be [R_0 500 m 30 deg]^T, where R_0 is the square distance of the UAV from the origin, at the initial time. Similar to the previous scenarios, simulations were carried out and the results are shown in Fig. 10.

Also, in this scheme, it is possible for the UAV to converge to a loitering circle with radius smaller/greater than the initial one. For the loitering radius of 1,500 and 4,500 m, simulations were carried out and the results are shown in Figs. 11 and 12, respectively. It can be seen from Figs. 11 and12 that the UAV has successfully converged to a loitering motion around the origin in both scenarios. Yet, it must be reminded that scheme #3 can fail if the UAV flies in the radial direction. Thus, it is recommended that one employs scheme #4 if a loitering motion is desirable.
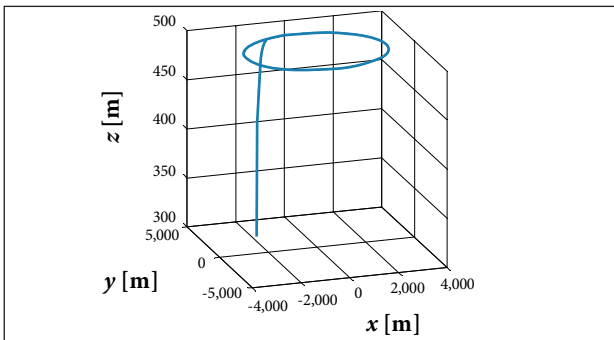
It is important to note that scheme #4 includes scenarios where the loitering radius can be smaller/greater than the initial distance of the UAV from the origin.

To verify the feasibility of scheme #4, a case study is developed in which the UAV is at the same initial condition as before. In the first example, let's assume that the UAV is desired to loiter around the origin with a radius of 1,500 m, a value smaller than its initial distance to the origin. For this case study, simulation results are shown in Fig. 13.
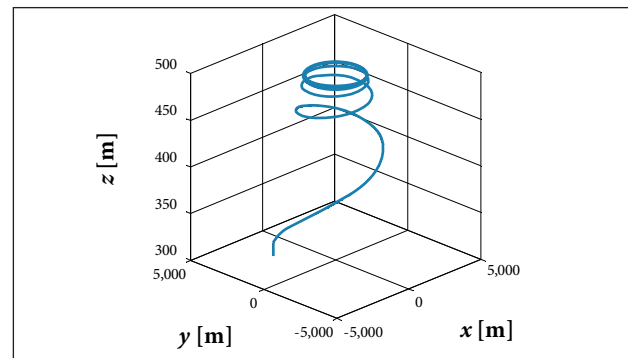

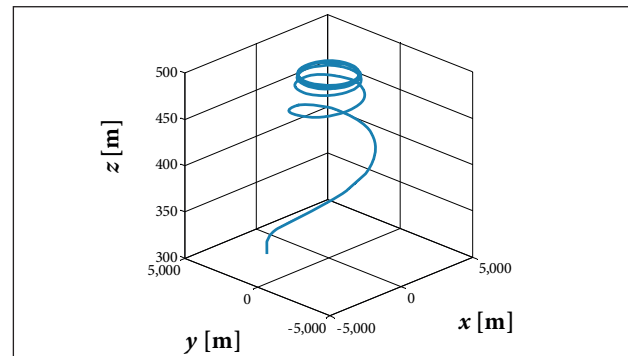Figure 10. UAV trajectory obtained from scheme #3 — first example.

Figure 11. UAV trajectory obtained from scheme #3 — second example.

Figure 8. UAV trajectory obtained from scheme #2.

Figure 9. Side-looking camera angle obtained from scheme #2.
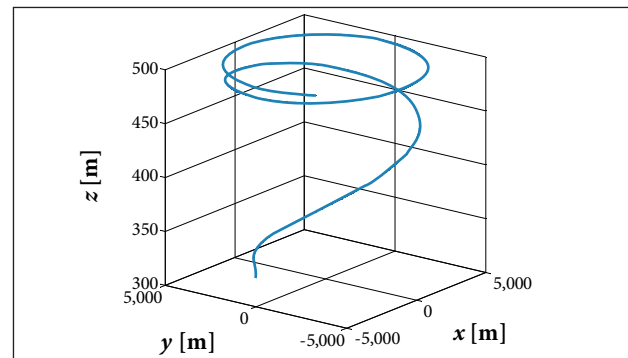

Figure 12. UAV trajectory obtained from scheme #3 — third example.

In Fig. 13, the first and the second phases of the path are shown in red and blue, respectively (see Fig. 4). As it can be seen from the figure, the UAV has successfully converged to the desired reference signal. In the second case study, assume that the UAV is desired to loiter around the origin with a radius of 4,000 m, a value greater than its initial distance to the origin. For this case study, simulation results are shown in Fig. 14, where the first and the second phases of the path are shown in red and the last phase is shown in blue (see Fig. 5). As it can be seen from Fig. 14, the UAV has successfully converged to a loitering motion around the origin with the desired loitering radius.
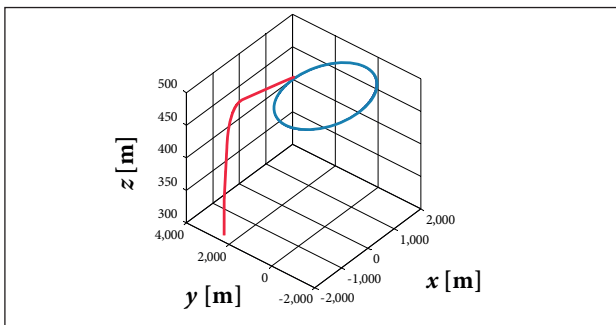

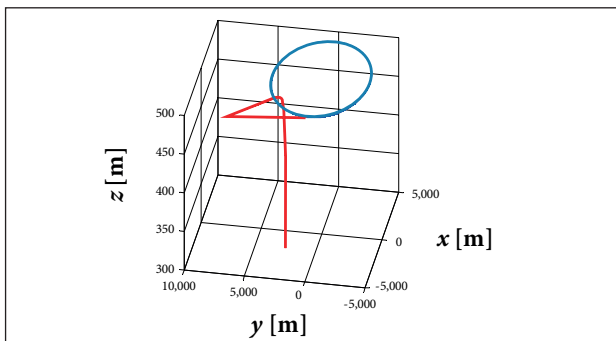**Figure 13.** UAV trajectory obtained from scheme #4 — first case study.

Figure 14. UAV trajectory obtained from scheme #4 — second case study.

CONCLUSION

In this paper, several feedback linearization schemes were studied to make a fixed-wing UAV, with constant forward velocity, (i) fly over or (ii) loiter around a stationary objective position. Throughout the paper, advantages and disadvantages of each scheme were discussed. A main drawback of the proposed schemes is that they do not take account of the maximum angular velocity constraint of fixed-wing UAVs. In scheme #1, the proposed method failed if the UAV was exactly above the objective position. Scheme #2 was disadvantageous in the sense that the loitering radius cannot be explicitly controlled. This was improved in scheme #3. Yet, the method in scheme #3 failed when the UAV had to fly radially inward or radially outward. However, if the heading of the UAV did not fall within this region, the UAV converged to a loitering motion around the origin. In scheme #4, the UAV had to be far enough from the objective circle. In this manner, one could assume that the UAV reaches the tangency point with its heading far from inward-outward direction, and therefore scheme #3 could bring the UAV to loiter around the objective position, with desirable radius. It is important to note that, in scheme #3 and scheme #4, the switching from a control strategy to another was given as an equality-type condition. Therefore, for real-world implementation, thresholds must be defined, and the equalities must be replaced by appropriate inequalities.

ACKNOWLEDGEMENTS

REFERENCES

Almurib HAF, Nathan PT, Kumar TN (2011) Control and path planning of quadrotor aerial vehicles for search and rescue. Proceedings of the IEEE SICE Annual Conference; Tokyo, Japan.

Beard RW, McLain TW, Nelson DB, Kingston D, Johanson D (2006) Decentralized cooperative aerial surveillance using fixed-wing miniature UAVs. Proc IEEE 94(7):1306-1324. doi: 10.1109/JPROC.2006.876930

Bonyan Khamseh H, Pimenta LCA, Tôrres LAB (2014) Decentralized coordination of constrained fixed-wing unmanned aerial vehicles: circular orbits. Proceedings of the IFAC World Congress; Cape Town, South Africa.

Casbeer DW, Kingston DB, Beard RW, McLain TW, Li SM, Mehra R (2006) Cooperative forest fire surveillance using a team of small unmanned air vehicles. Int J Syst Sci 37(6)351-360. doi: 10.1080/00207720500438480

Costa FG, Ueyama J, Braun T, Pessin G, Osório FS, Vargas PA (2012) The use of unmanned aerial vehicles and wireless sensor network in agricultural applications. Proceedings of the IEEE International Geoscience and Remote Sensing Symposium; Munich, Germany.

Fan W, Zhiyong G (2009) An approach to formation maneuvers of multiple nonholonomic agents using passivity techniques. Proceedings of the Chinese Control and Decision Conference; Guilin, China.

Frew E, Lawrence D, Morris S (2008) Coordinated standoff tracking of moving targets using Lyapunov guidance vector fields. J Guid Contr Dynam 31(2):290-306. doi: 10.2514/1.30507

Gonçalves MM, Pimenta LCA, Pereira GAS (2011) Coverage of curves in 3D with swarms of nonholonomic aerial robots. Proceedings of the IFAC World Congress; Milano, Italy.

Gonçalves VM, Pimenta LCA, Maia CA, Dutra BCO, Pereira GAS (2010) Vector fields for robot navigation along time-varying curves in n-dimensions. IEEE Trans Robot26(4):647-659. doi: 10.1109/TRO.2010.2053077

Hafez AT, Marasco AJ, Givigi AN, Beaulieu A, Rabbath CA (2013) Encirclement of multiple targets using model predictive control. Proceedings of the American Control Conference; Washington, USA.

Hsieh MA, Kumar V, Chaimowicz L (2008) Decentralized controllers for shape generation with robotic systems. Robotica 26(5):691-701. doi: 10.1017/S0263574708004323

Hsieh MA, Loizou S, Kumar RV (2007) Stabilization of multiple robots on stable orbits via local sensing. Proceedings of the IEEE International Conference on Robotics and Automation; Rome, Italy.

Kanchanavally S, Ordonez R, Schumacher CJ (2006) Path planning in three dimensional environment using feedback linearization. Proceedings of the American Control Conference; Minneapolis, USA.

Li H, Wang B, Liu L, Tian G, Zheng T, Zhang J (2013) The design and application of SmartCopter: an unmanned helicopter based robot for transmission line inspection. Proceedings of the Chinese Automation Congress; Changsha, China.

Marasco AJ, Givigi SN, Rabbath CA (2012) Model predictive control for the dynamic encirclement of a target. Proceedings of the American Control Conference; Montreal, Canada.